Stem Cell Research & Therapy

RESEARCH

Open Access

CHD7 regulates definitive endodermal and mesodermal development from human embryonic stem cells

Rong Hu[1†], Jin Zhao[1†], Kuan Chen Lai[1], Shikun Wang[1], Jianqing Zheng[1], Christopher Stoddard[2] and Laijun Lai[1,3,4*]

Abstract

Background CHD7 encodes an ATP-dependent chromodomain helicase DNA binding protein; mutations in this gene lead to multiple developmental disorders, including CHARGE (Coloboma, Heart defects, Atresia of the choanae, Retardation of growth and development, Genital hypoplasia, and Ear anomalies) syndrome. How the mutations cause multiple defects remains largely unclear. Embryonic definitive endoderm (DE) generates the epithelial compartment of vital organs such as the thymus, liver, pancreas, and intestine.

Methods In this study, we used the clustered regularly interspaced short palindromic repeats (CRISPR)/Cas9 technique to delete the CHD7 gene in human embryonic stem cells (hESCs) to generate CHD7 homozygous mutant ($CHD7^{-/-}$), heterozygous mutant ($CHD7^{+/-}$), and control wild-type ($CHD7^{+/+}$) cells. We then investigated the ability of the hESCs to develop into DE and the other two germ layers, mesoderm and ectoderm in vitro. We also compared global gene expression and chromatin accessibility among the hESC-DE cells by RNA sequencing (RNA-seq) and the assay for transposase-accessible chromatin with sequencing (ATAC-seq).

Results We found that deletion of CHD7 led to reduced capacity to develop into DE and mesoderm in a dose-dependent manner. Loss of CHD7 led to significant changes in the expression and chromatin accessibility of genes associated with several pathways. We identified 40 genes that were highly down-regulated in both the expression and chromatin accessibility in CHD7 deleted hESC-DE cells.

Conclusions CHD7 is critical for DE and mesodermal development from hESCs. Our results provide new insights into the mechanisms by which CHD7 mutations cause multiple congenital anomalies.

Keywords CHD7, CHARGE syndrome, Human embryonic stem cells, Definitive endoderm

[†]Rong Hu and Jin Zhao contributed equally to this work.

*Correspondence:
Laijun Lai
laijun.lai@uconn.edu
[1]Department of Allied Health Sciences, University of Connecticut, 1390 Storrs Road, Storrs 06269, CT, USA
[2]Department of Department of Genetics and Genome Sciences, University of Connecticut Health, Farmington, CT, USA
[3]Institute for Systems Genomics, University of Connecticut, Storrs, CT, USA
[4]University of Connecticut Stem Cell Institute, University of Connecticut, Storrs, CT, USA

Background

CHARGE syndrome is a complex genetic disease with an occurrence of approximately 1 per 10,000 live births worldwide [1–3]. CHARGE represents an acronym for Coloboma, Heart defects, Atresia of the choanae, Retardation of growth and development, Genital hypoplasia, and Ear anomalies. De novo mutations of chromodomain helicase DNA-binding 7 (CHD7) are a major cause of CHARGE syndrome [1, 2, 4–16]. The mutations are distributed along the coding region of CHD7, and most are nonsense, or frameshift mutations leading to the loss of function [4, 17]. CHD7 mutations are also associated with idiopathic hypogonadotropic hypogonadism, Kallmann syndrome, autism spectrum disorders, DiGeorge syndrome, and non-syndromic patients with congenital heart defects [18–21].

CHD7 is a chromatin remodeling factor that regulates access to DNA by using the energy of ATP hydrolysis to alter nucleosome structure (22, 23). The human CHD7 spans approximately 189 kb at chromosome 8 and contains 38 exons encoding for a large protein (2997 aa, about 336 kD). CHD7 contains tandem N-terminal chromodomains that mediate binding to methylated histones, a central SNF2-like ATPase/helicase domain that may mediate chromatin remodeling, a histone/DNA-binding SANT domain, and two C-terminal BRK domains of unknown function [17]. CHD7 protein has a cell type-specific and lineage stage-specific function in regulating the expression of other developmental genes [4, 14, 15, 22, 23].

CHD7 is expressed widely during development and remains ubiquitous in later stages of fetal development [23, 24]. However, CHD7 has no effect on embryonic stem cell (ESC) pluripotency, self-renewal, or reprogramming [4, 17]. Mice with homozygous loss-of-function mutation of CHD7 die at E10.5-E11.5; heterozygous CHD7 mutant mice display some features of human CHARGE syndrome including multisystem developmental defects [24–26].

It has been reported that CHARGE syndrome is more complex than the acronym describes, with other systems involved including the immune system [1, 7–13]. CHARGE patients usually experience recurrent infections and have T cell lymphopenia, which is due to thymic hypo/aplasia [1, 13]. The thymus is the primary organ for T cell generation. T cell development in the thymus is dependent on the thymic microenvironment, in which thymic epithelial cells (TECs) are the major component [27–35]. Studies on thymus organogenesis in the murine embryo have indicated that TECs arise from thymic epithelial progenitors (TEPs) that originate from DE [36, 37]. It is unclear whether thymic hypo/aplasia in CHARGE syndrome is caused by a defect in DE and/or subsequent development. The CHD7 target genes in DE also remain unclear.

It is well known that hESCs can either propagate indefinitely in vitro in an undifferentiated state or differentiate into all three germ layers. In this study, we used the CRISPR/Cas9 technique to delete the CHD7 gene in hESCs to generate CHD7$^{-/-}$, CHD7$^{+/-}$, and control wild-type CHD7$^{+/+}$ cells. We then determined the capacity of the hESCs to develop into DE and compared global gene expression and chromatin accessibility among CHD7$^{-/-}$, CHD7$^{+/-}$, and CHD7$^{+/+}$ hESC-DE by RNA-seq and ATAC-seq.

We found that loss of CHD7 led to reduced ability to develop into DE in a dose-dependent manner, which was related to alteration of expression and open chromatin structure of genes associated with several pathways. We identified 40 genes that had both highly reduced expression and chromatin accessibility in CHD7 deleted hESC-DE cells; 13 of them were zinc finger proteins (ZNFs) in the generic transcription pathway and long intergenic non-coding RNA (lincRNA) genes.

Although CHARGE patients have multisystem developmental defects, how the CHD7 mutations lead to multiple defects remains largely unknown. Therefore, we also determined the ability of CHD7$^{-/-}$, CHD7$^{+/-}$, and CHD7$^{+/+}$ hESCs to develop into mesoderm and ectoderm. We found that loss of CHD7 also led to reduced ability to develop into mesoderm in a dose-dependent manner. Our studies provide new insights into CHARGE pathogenesis.

Materials and methods

The deletion of the CHD7 gene in hESCs

Two guide RNAs (gRNAs) were chosen that flanked exon3 of the CHD7 gene using available guide RNA design tools (http://www.rgenome.net/cas-designer/ and https://chopchop.cbu.uib.no/). The guide RNA was cloned into pSpCas9(BB)-2 A-Puro (PX459) V2.0 (a gift from Feng Zhang, Addgene plasmid # 62988) using plasmid digested with bbs1 to allow for ligation of the guide RNA insert. H9 hESCs (obtained from WiCell Research Institute, https://www.wicell.org/home/stem-cells/catalog-of-stem-cell-lines/wa09.cmsx) were grown on mitotically inactivated MEFs. Twenty-four hours prior to targeting, cells were treated with ROCKi (Y-27632). The following day the cells were singleized with accutase and pelleted. Cells were resuspended according to the protocol provided in the LONZA 4D nucleofection Primary P3 kit. The CRISPR plasmids (2 ug each) were added to the nucleofection solution. The cells were nucleofected and then plated on DR4 MEFs supplemented with ROCKi. The following day 0.5-1 ng/μl of puromycin and ROCKi was added to fresh media. This selection continued to select cells that were puromycin resistant and

contained the plasmids. ROCKi was kept in the cells until small colonies were observed. After a total of 15 days colonies were transferred into 24 well plates. Four days later, a few colonies from each well were isolated and DNA extracted using the HOT SHOT method to prepare template for PCR. PCR was performed across the deleted region. After several rounds of PCR screening, selected CHD7$^{-/-}$, CHD7$^{+/-}$, and CHD7$^{+/+}$ clones were transferred to mTeSR™ Plus medium (STEMCELL Technologies, Vancouver, Canada) in culture plates coated Corning™ Matrigel™ hESC-Qualified Matrix (Corning, Tewksbury, MA).

Inducing the differentiation of hESCs into DE, mesoderm, and endoderm

hESCs were induced to generate DE by the PSC Definitive Endoderm Induction Kit (Thermo Fisher Scientific, Rockford, IL) according to the manufacturer's instructions. hESCs were induced to differentiate into ectoderm or mesoderm by the STEMdiff™ Trilineage Differentiation Kit (STEMCELL Technologies).

Immunofluorescence

Immunofluorescent analysis of cells was performed as described [38, 39]. Briefly, cells were fixed with 4% paraformaldehyde for 10 min, permeabilized with 0.1% Triton™ X-100 for 15 min and blocked with 2% BSA for 1 h at room temperature. The cells were stained with the Human Embryonic Stem Cell Marker Panel containing anti-OCT4, NANOG, TRA-1-60R, SSEA4 antibodies (Abcam, Cambridge, UK), or DE markers including anti-FOXA2, SOX17 (Thermo Fisher), and anti-CXCR4 antibodies (Abcam). Alexa Fluor® 488 or 546 labeled goat anti-rabbit and mouse IgG H&L (Thermo Fisher or Abcam) were used as the secondary antibody. DAPI was used as a counterstain. The cells were observed under a Nikon A1R Spectral Confocal microscope (Nikon, Kanagawa, Japan) or Keyence microscope (KEYENCE, USA).

Flow cytometry

Single-cell suspensions of cells were permeabilized with a Cytofix/Cytoperm solution at 4℃ (BD Biosciences, San Jose, CA). The cells were then stained with FITC-conjugated anti-Ki67 antibody (BioLegend) or anti-cleaved caspase-3 antibody (Cell Signaling, Danvers, MA), followed by a fluorochrome-conjugated second antibody. The cells were analyzed on a LSR II flow cytometer (BD Biosciences); data analysis was done using FlowJo software (Ashland, OR).

Real-time qualitative RT-PCR (qRT-PCR)

Total RNA from cells was isolated from cells, and cDNA was synthesized as described [40]. Equal amounts of cDNA were used for RT-PCR. qRT-PCRs were performed with the Power SYBR green mastermix (Applied Biosystems, UK) using the 7500 real-time PCR system (Applied Biosystems, UK) [41]. After normalization to GAPDH, samples were plotted relative to control protein-treated group. Primers are summarized in Supplemental Table 1.

Alkaline phosphatase (AP) staining

hESCs were stained by AP Staining Kit (Red color) according to the manufacturer's instructions (Abcam).

Western blot

Cells were washed with PBS, resuspended in a sample buffer, loaded on SDS-PAGE, transferred to a polyvinylidene fluoride membrane that was incubated with rabbit anti-CHD7 antibody (Novus Biologicals, Centennial, CO), followed by HRP conjugated anti-rabbit IgG secondary antibody. The Western Blot was developed with Super Signal® West Pico chemiluminescent Substrate (Thermo Fisher).

RNA-seq

Total RNA was isolated from cells by the NucleoSpin RNA Mini kit (Macherey-Nagel, USA). RNA-seq libraries were prepared using an RNA-seq preparation kit (Illumina, Inc.). An Illumina NovaSeq 6000 was used for sequencing. Quality control of raw reads was conducted using FastQC. The reads were trimmed using Trimmomatic. Afterward, the paired-end raw reads were aligned to the human reference genome (hg38) using HISAT2 and sorted by Samtools. Mapped reads were performed using htseq-count. Differentially expressed genes between groups were analyzed using the "DEseq2" package in the R with the input data of count matrix. Visualizations of the principal component plot of the samples, volcano plot of the samples with log2FoldChange and -log10 adjusted *P*value (padj), heatmap of the gene expression with Z-Score were generated using the same package in the R. Genes with padj < 0.05 were selected as the criteria for significant differences. The significant differential genes were anlayzed for functional pathway analysis by Ingenuity pathway analysis (IPA).

ATAC-seq

hESC-DE cells were sorted from cultured cells and 50,000 cells for each sample were lysed using an adjusted lysis buffer based on the Omni-ATAC protocol, followed by a transposition reaction with hyperactive Tn5 transposase. The DNA fragments were purified using the MinElute Reaction Cleanup Kit (Qiagen, Germantown, MD). Library construction was performed according to the manufacturer's recommendations of the Nextera DNA Prep Kit. Libraries were purified using AMPure

XP beads to remove primer dimers. The library quality was evaluated using the TapeStation D1000 ScreenTape. Libraries were sequenced on an Illumina platform with a read length configuration of 150 bp paired-end, generating 30 million paired-end reads per sample (30 million in each direction).

Raw sequencing data was first filtered by fastp, low-quality reads were discarded, and the reads contaminated with adaptor sequences were trimmed. Clean Reads were further treated with MarkDuplicates to eliminate duplication bias introduced in library preparation and sequencing. Reads were first mapped to the reference genome of hg38 using Bowtie2 with default parameters. The MACS2 was used for peak calling. The ChIPseeker was used for peak annotation and peak distribution analysis. The differential binding peaks were identified by DiffBind; the peaks with false discovery rate (FDR) under 0.05 and absolute value of Log2 Fold Change > 1 or <-1 were regarded as significant differential peaks. These significant differential peaks located genes were used for functional pathway analysis by IPA. Scatter plot for combing the RNA-seq and ATAC-seq with log2FoldChange was performed by ggplot2.

Statistical analysis

P-values for two groups were based on the two-sided Student's t test. For comparing means of multiple groups, significance was determined using one-way ANOVA with Dunnett test, or two-way ANOVA with Tukey test. A confidence level above 95% ($p < 0.05$) was determined to be significant.

Results

Generation and characterization of CHD7$^{-/-}$, CHD7$^{+/-}$, and CHD7$^{+/+}$ hESCs

We knocked out the CHD7 gene in H9 hESCs by the CRISPR/Cas9 technique using two gRNAs that flanked the CHD7 exon 3 [exon 2 contains the ATG start codon [25]. We transfected hESCs with plasmids containing the CHD7 gRNAs and then selected positive cells with puromycin (the plasmids contain puromycin N-acetyl-transferase). The positive clones were first screened by PCR with primers 1 F and 1R (Supplemental Fig. 1 and Supplemental Table 1). The clones with a 600 bp PCR product had at least one allele with exon 3 deleted and were CHD7$^{+/-}$ or CHD7$^{-/-}$ (Supplemental Fig. 2). The 1366 bp band in CHD7$^{+/+}$ clones did not show up because the PCR extension was not long enough to amplify this size band. The clones with the 600 bp PCR product were further screened with primers 2 F and 2R to identify clones with one allele intact. Supplemental Fig. 3 shows that clones 5, 6, 8, 11, 15, 18, 19, and 21 lacked exon 3 in the genome and were CHD7$^{-/-}$ and that clones 2, 20, and 22 had an intact exon 3 and were CHD7$^{+/-}$. Clones 5, 11, 15 and 21 (CHD7$^{-/-}$) and clones 2 and 20 (CHD7$^{+/-}$) were further expanded and characterized. The DNA sequences of CHD7$^{+/+}$, CHD7$^{+/-}$ (clone 2 with mutations in one allele) and CHD7$^{-/-}$ (clone 11 with mutations in two alleles) are shown in Fig. 1A. The mutations resulted in a frameshift of the CHD7 coding sequences, which created an early termination and truncation of the CHD7, leading to low or absent CHD7 protein in the CHD7$^{+/-}$, or CHD7$^{-/-}$ hESCs as compared to CHD7$^{+/+}$ hESCs (Fig. 1B and Supplemental Fig. 4).

No Significantly morphological differences were observed among the CHD7$^{-/-}$, CHD7$^{+/-}$ and CHD7$^{+/+}$ hESCs (Fig. 1C). We then examined the expression of pluripotent markers in these hESCs. All the CHD7$^{-/-}$, CHD7$^{+/-}$ and CHD7$^{+/+}$ hESCs expressed the pluripotency marker alkaline phosphatase (AP) (Fig. 1D). Immunofluorescence showed that they also expressed other pluripotency markers including SSEA4, OCT4 NANOG, and TRA-1-60R (Fig. 1E). The data indicate that the hESCs were undifferentiated.

We also determined whether the CHD7 deletion affected hESC proliferation and survival. The undifferentiated hESCs were analyzed for Ki67^{+} or BrdU $^{+}$ proliferating cells and there were no significant differences among the CHD7$^{-/-}$, CHD7$^{+/-}$ and CHD7$^{+/+}$ hESCs (Fig. 1F, G, and Supplemental Fig. 5A). Furthermore, the percentages of cleaved caspase-3^{+} and Annexin V^{+} apoptotic cells among the hESCs were also not significantly different (Fig. 1H, I, and Supplemental Fig. 5B). Collectively, our results suggest that CHD7 deficiency does not affect the pluripotency, self-renewal, survival and proliferation of undifferentiated hESCs.

Deletion of CHD7 leads to reduced ability of hESCs to differentiate into DE cells in vitro

We then investigated the ability of CHD7$^{+/-}$ and CHD7$^{-/-}$ hESCs to develop into DE in vitro, as compared to CHD7$^{+/+}$ hESCs. An equal number of CHD7$^{+/-}$, CHD7$^{-/-}$ and CHD7$^{+/+}$ hESCs were induced to differentiate into DE by the PSC definitive endoderm induction Kit. After differentiation, the cells were analyzed for the expression of the DE markers SOX17, CXCR4, and FOXA2 by immunofluorescence. We found that most of CHD7$^{+/+}$ hESC-derived cells expressed SOX17, CXCR4 and FOXA2, indicating that the DE had been generated from CHD7$^{+/+}$ hESCs (Fig. 2A). In contrast, the percentages of CHD7$^{+/-}$ hESC-derived cells expressing SOX17, CXCR4, and FOXA2 were lower than those of CHD7$^{+/+}$ hESCs-derived cells, and the percentages of CHD7$^{-/-}$ hESC-DE cells expressing these markers were lower than those of CHD7$^{+/-}$ hESC-derived cells (Fig. 2A-F). Because an antibody against goosecoid (GSC), another marker for DE, was not commercially available, we used real-time quantitative RT-PCR (qRT-PCR) to detect the mRNA

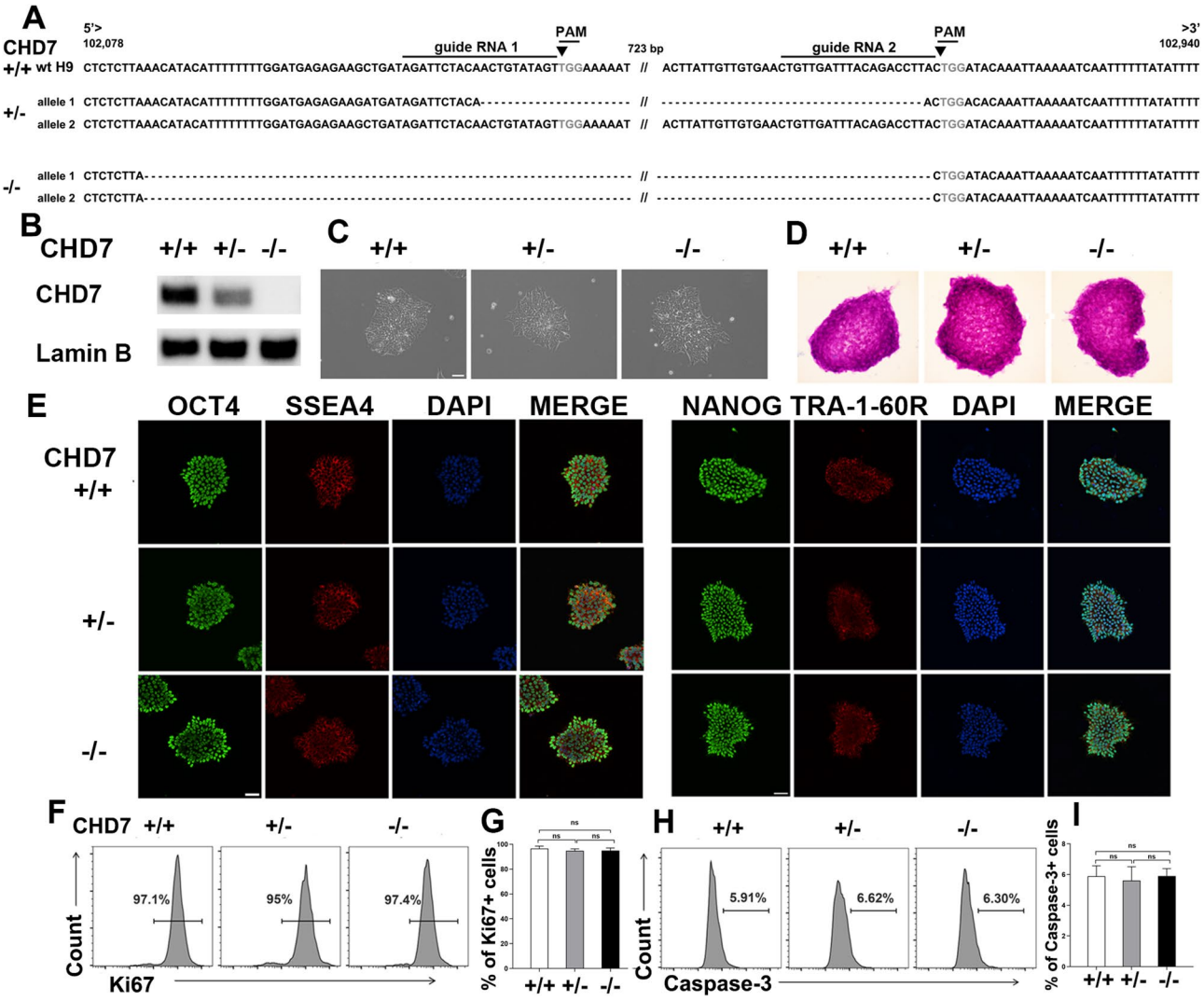

Fig. 1 The generation and characterization of CHD7$^{-/-}$, CHD7$^{+/-}$ and CHD7$^{+/+}$ hESCs. (**A**) The exon 3 of CHD7 was PCR-amplified and sequenced. Sequences of WT (CHD7$^{+/+}$), and both alleles from CHD7$^{+/-}$ (clone 2) and CHD7$^{-/-}$ (clone 11) are shown. (**B**) Western blot with an anti-CHD7 antibody showing CHD7 protein expression in CHD7$^{+/+}$, CHD7$^{+/-}$, and CHD7$^{-/-}$ hESCs. Lamin B was used as a loading control. Full-length blots are presented in Supplemental Fig. 4. (**C**) The morphology of the hESCs observed under a reversed microscope. (**D**, **E**) The undifferentiated state of the hESCs was confirmed by their expression of pluripotency markers (**D**) AP, (**E**) SSEA4, OCT4 NANOG, and TRA-1-60R detected by immunofluorescence. (**F**) Representative flow cytometric profiles and (**G**) statistical analysis for the percentages of Ki67^{+} proliferating cells. (**H**) Representative flow cytometric profiles and (**I**) statistical analysis for the percentages of caspase 3^{+} apoptotic cells among the hESCs. (**G**, **I**) The data are expressed as mean + SD from three independent experiments. ns: no significant difference

level. Similarly, the expression level of GSC in CHD7$^{+/-}$ hESC-DE cells was lower than in CHD7$^{+/+}$ hESC-DE cells, and GSC expression in CHD7$^{-/-}$ hESC-DE cells was lower than in CHD7$^{+/-}$ hESC-DE cells (Fig. 2G). Taken together, our results suggest that CHD7 deficient hESCs have a defect in developing into DE which is dosage dependent.

We also investigated whether the defect in developing into DE was due to decreased cell survival and/or proliferation of hESC-DE cells. For cell proliferation, Ki67^{+} or BrdU $^{+}$ proliferating cells among CHD7$^{+/-}$, CHD7$^{-/-}$ and CHD7$^{+/+}$ hESC-DE cells were analyzed. The percentage of Ki67^{+} or BrdU $^{+}$ proliferating cells among CHD7$^{+/-}$, CHD7$^{-/-}$ and CHD7$^{+/+}$ hESC-DE cells were not significantly different (Fig. 2H, I, and Supplemental Fig. 5C), suggesting CHD7 deficiency did not affect the proliferative ability of hESC-DE cells. In contrast, the percentage of caspase 3^{+} or annexin V^{+} apoptotic cells as well as propidium iodide (PI)$^{+}$ dead cells in CHD7$^{-/-}$ and CHD7$^{+/-}$ hESC-DE were significantly higher than those in CHD7$^{+/+}$ hESC-DE (Fig. 2J, K, and Supplemental Fig. 5D, E). In contrast, the percentage of Annexin V^{-} PI^{-} viable cells in CHD7$^{-/-}$ and CHD7$^{+/-}$ hESC-DE were significantly lower than that in CHD7$^{+/+}$ hESC-DE

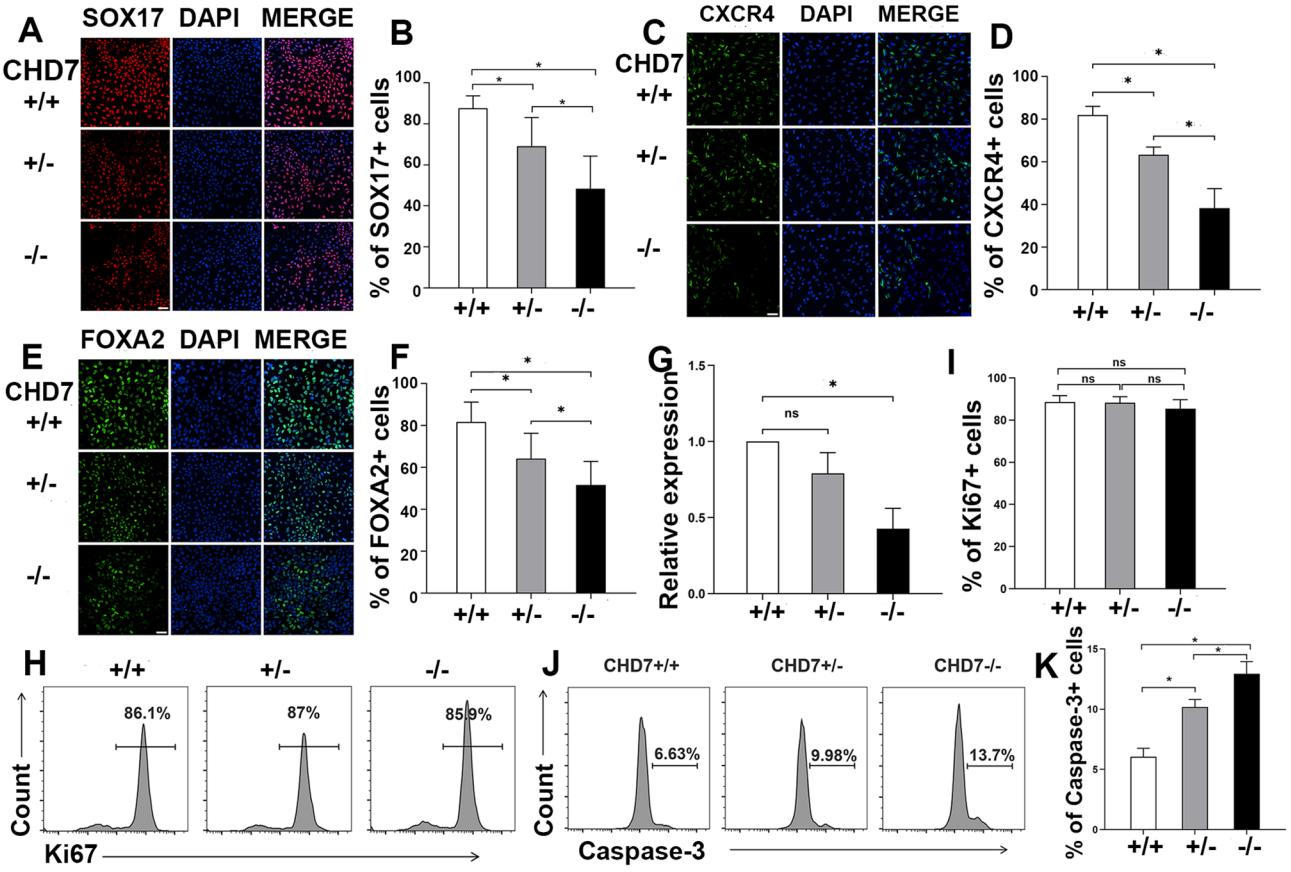

Fig. 2 CHD7 deficient hESCs have a defect in developing into DE. CHD7$^{+/+}$, CHD7$^{+/-}$, and CHD7$^{-/-}$ hESCs (5×10^5 cells/well) were induced to differentiate into DE. On day 6, (**A-F**) the expression of SOX17, CXCR4, and FOXA2 in the hESC-DE cells was analyzed by immunofluorescence. (**A**, **C**, **E**) Representative immunofluorescent images and (**B**, **D**, **F**) statistical analysis for the percentages of SOX17, CXCR4, and FOXA2 positive cells in DE cells. (**G**) Relative expression levels of GSC in CHD7$^{+/+}$, CHD7$^{+/-}$, and CHD7$^{-/-}$ hESC-DE cells were analyzed by qRT-PCR. The expression level of GSC in CHD7$^{+/+}$ hESC-DE was defined as 1. (**H**) Representative flow cytometric profiles and (**I**) statistical analysis for the percentages of Ki67$^+$ proliferating cells. (**J**) Representative flow cytometric profiles and (K) statistical analysis for the percentages of caspase 3$^+$ apoptotic cells among the hESC-DE cells. (B, D, F, G, I, K) The data are expressed as mean + SD from three independent experiments. * $P < 0.05$, compared with CHD7$^{+/+}$group

(Supplemental Fig. 5F). The results suggest that CHD7$^{-/-}$ and CHD7$^{+/-}$ hESC-DE cells have a defect in cell survival. Although we only show the results from Clone 11 for CHD7$^{-/-}$ and clone 2 for CHD7$^{+/-}$ cells, we obtained similar results with Clones 5, 15 and 21 for CHD7$^{-/-}$ and clone 20 for CHD7$^{+/-}$ hESCs. Collectively, our results suggest that CHD7 deficient hESCs have a defect in developing into DE, which is likely due to reduced survival of DE cells.

Deletion of CHD7 leads to significant changes in global gene expression in hESC-DE cells

To find the molecular basis of the defect in developing into DE from CHD7 deficient hESCs, we performed transcriptome profiling and compared global gene expressions among CHD7$^{+/+}$, CHD7$^{+/-}$, and CHD7$^{-/-}$ hESC-DE cells by RNA-seq. The RNA-seq data confirmed a significant decrease in CHD7 transcripts according to their genotypes in *CHD7*$^{+/-}$ and CHD7$^{-/-}$ hESC-DE, as compared to CHD7$^{+/+}$ hESC-DE, consistent with the data for CHD7 protein expression levels detected by Western blot (Fig. 1B). Principal component (PC) analysis (PCA) of the RNA-seq data revealed a clear separation of genotypes along PC1 and PC2, suggesting that deletion of CHD7 led to significant changes in global gene expression (Fig. 3A).

Among the differentially expressed genes between CHD7$^{+/+}$ and CHD7$^{-/-}$ hESC-DE [1708 genes, Padj < 0.05], 182 genes were highly up-regulated, and 183 genes were highly down-regulated in CHD7$^{-/-}$ hESC-DE based on the criteria log2 fold change > 1 or <-1 and Padj < 0.05 (Fig. 3B). Among those between CHD7$^{+/+}$ and CHD7$^{+/-}$ hESC-DE (668 genes, Padj < 0.05), 113 genes were highly up-regulated, and 72 genes were highly down-regulated in CHD7$^{-/-}$ hESC-DE (Supplemental Fig. 6). Among those between CHD7$^{+/-}$ and CHD7$^{-/-}$ hESC-DE (751 genes, Padj < 0.05), 63 genes were highly up-regulated, and 79 genes were highly down-regulated

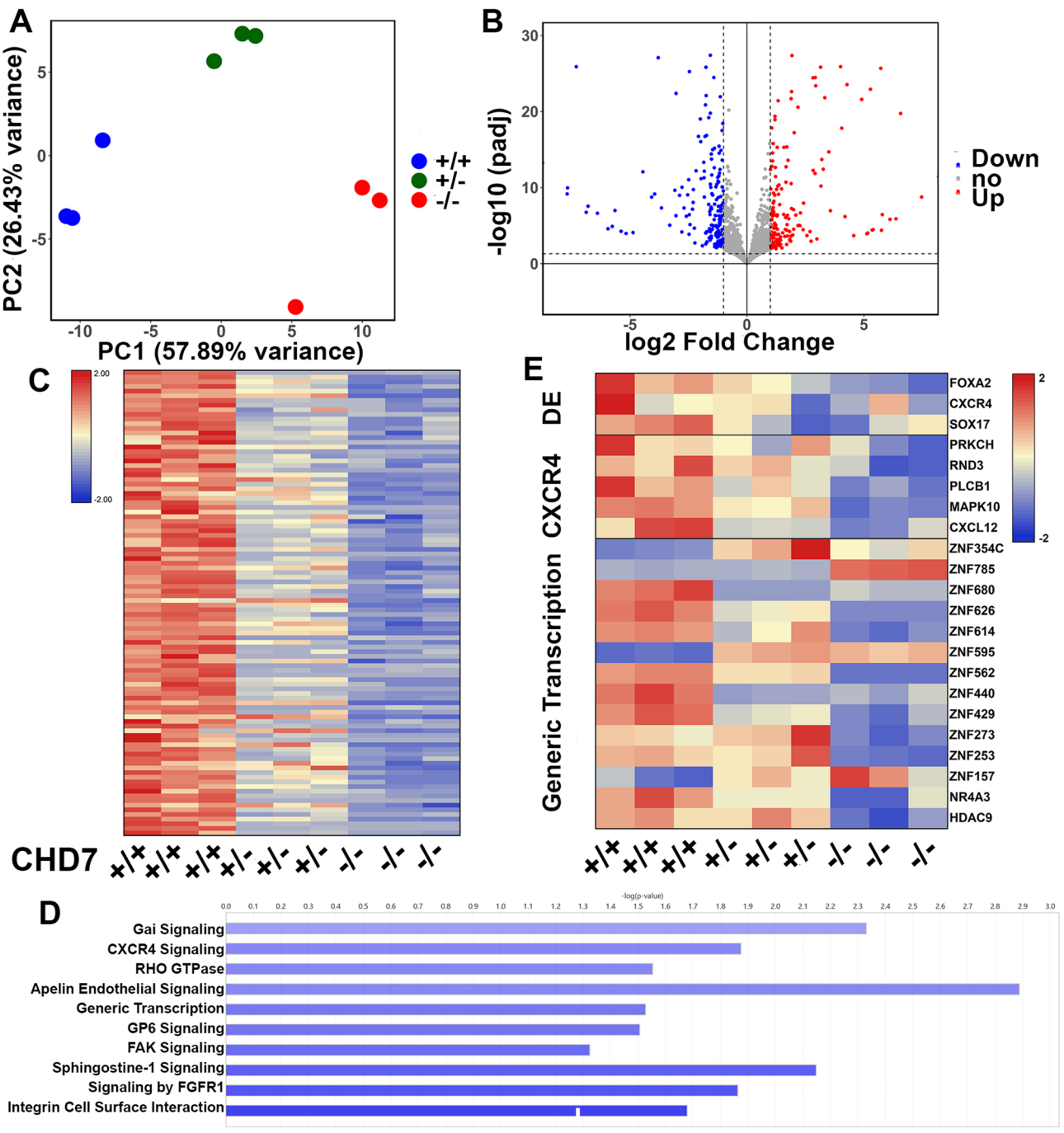

Fig. 3 CHD7 deletion in hESC-DE leads to significant changes in global gene expression. CHD7$^{+/+}$, CHD7$^{+/-}$, and CHD7$^{-/-}$ hESCs were induced to differentiate into DE as in Fig. 2. On day 6, CXCR4^{+} DE cells were sorted from the cultures. RNAs were extracted from the sorted cells and analyzed for global gene expression by RNA-seq. (**A**) PCA of RNA-seq data showing PC1 and PC2 among CHD7$^{+/+,}$ CHD7$^{+/-}$, and CHD7$^{-/-}$ hESC-DE groups. (**B**) Volcano plot showing gene expression changes between CHD7$^{+/+}$ and CHD7$^{-/-}$ hESC-DE groups. Red color: up-regulated; blue color: down-regulated; gray color: not significant. (**C**) Heatmap showing significantly downregulated genes in CHD7$^{-/-}$ hESC-DE cells as compared to CHD7$^{+/+}$ and CHD7$^{+/-}$hESC-DE cells. The color scale is shown on the right. (**D**) IPA of significantly downregulated pathways in CHD7$^{-/-}$ hESC-DE cells as compared to CHD7$^{+/+}$ hESC-DE cells. (**E**) Heatmap showing the expression levels of genes related to DE cells, CXCR4 signaling and generic transcriptional pathways among CHD7$^{+/+,}$ CHD7$^{+/-}$, and CHD7$^{-/-}$ hESC-DE groups. $n = 3$ CHD7$^{+/+}$, $n = 3$ CHD7$^{+/-}$, and $n = 3$ CHD7$^{-/-}$ group

in CHD7$^{-/-}$ hESC-DE based on the criteria above (Supplemental Fig. 7). Our results are consistent with previous reports that CHD7 both positively and negatively regulates expression of other genes [42–44].

Heatmap revealed that the downregulated genes in CHD7$^{+/-}$ and CHD7$^{-/-}$ hESC-DE cells as compared with CHD7$^{+/+}$ hESC-DE cells had a dose-dependence (Fig. 3C). IPA revealed that the down-regulated genes in CHD7$^{-/-}$ hESC-DE cells were involved in Gαi signaling, CXCR4 signaling, signaling by Rho family GTPases, apelin endothelial signaling, generic transcription, GP6 signaling, FAK signaling, sphingosine-1-phosphate signaling, signaling by FGFR1 and integrin cell surface interaction pathways (Fig. 3D, E). Within the generic transcription pathway, 11 genes were down-regulated, and 3 genes were up-regulated (Fig. 3E); most of them were zinc finger proteins (ZNFs).

Deletion of CHD7 alters chromatin accessibility in hESC-DE cells in differentially expressed genes

Since CHD7 uses the energy of ATP hydrolysis to evict, slide, or rearrange nucleosomes on chromatin [42, 45], we used ATAC-seq to investigate genome wide mapping of chromatin accessibility among CHD7$^{+/+}$, CHD7$^{+/-}$, CHD7$^{-/-}$ DE cells and to compare peaks across genotypes. ATAC-seq peaks corresponded to regions of open chromatin; each peak was annotated by the nearest gene. PCA of the ATAC-seq data also revealed a clear separation of genotypes along PC1 and PC2, suggesting that consistency was across replicates and deletion of CHD7 significantly altered chromatin accessibility in hESC-DE (Fig. 4A).

Significantly differential peaks, also known as differentially accessible regions, between CHD7$^{+/+}$ and CHD7$^{-/-}$ DE cells, CHD7$^{+/+}$ and CHD7$^{+/-}$, CHD7$^{+/-}$ and CHD7$^{-/-}$, and were 1,599, 642, and 385, respectively based on log2 fold change > 1 or <-1 and false discovery rate (FDR) < 0.05. Among the significantly differential peaks between CHD7$^{+/+}$ and CHD7$^{-/-}$ hESC-DE, 826 genes had reduced chromatin accessibility, and 773 genes had increased chromatin accessibility (Fig. 4B). Among the significantly differential peaks between CHD7$^{+/+}$ and CHD7$^{+/-}$ hESC-DE, 318 genes had reduced chromatin accessibility, and 324 genes had increased chromatin accessibility (Supplemental Fig. 8). Among the significantly differential peaks between CHD7$^{+/-}$ and CHD7$^{-/-}$ hESC-DE, 154 genes had reduced chromatin accessibility, and 231 genes had increased chromatin accessibility (Supplemental Fig. 9). Our results suggest that CHD7 can both increase and decrease chromatin accessibility in hESC-DE cells.

Peak differential analysis among CHD7$^{+/+}$, CHD7$^{+/-}$, and CHD7$^{-/-}$ hESC-DE cells showed that most of the differential peaks fell into enhancer regions (distal intergenic and intronic regions) (Fig. 4C). Our results are consistent with the previous reports that CHD7 preferentially binds to enhancers in ESC and other cells [17, 18, 23, 44, 46, 47]. Like the RNA-seq data (Fig. 3C), ATAC-seq heatmap revealed that the reduced chromatin accessibility in CHD7$^{+/-}$ and CHD7$^{-/-}$ hESC-DE cells as compared to CHD7$^{+/+}$ hESC-DE cells in a dose-dependent manner (Fig. 4D). IPA revealed that the pathways with reduced chromatin accessibility in CHD7$^{-/-}$ hESC-DE cells included generic transcription, Gαi signaling, and Rho family GTPases (Fig. 4E), which were overlapped with reduced gene expression pathways in the RNA-seq data (Fig. 3E). Among the generic transcription pathway, most of down-regulated genes were also ZNFs (Fig. 4F).

To identify misregulated genes whose enhancers were also differentially accessible in CHD7$^{-/-}$ hESC-DE cells, we integrated the RNA-seq and ATAC-seq data. We created a scatterplot using log2 fold changes for all peak/gene combinations from this combined analysis (Fig. 4G). We were particularly interested in the genes that had both downregulated expression and reduced chromatin accessible in CHD7$^{-/-}$ hESC-DE cells. Overall, 40 highly down-regulated genes in CHD7$^{-/-}$ DE cells versus CHD7$^{+/+}$ DE cells also had highly reduced chromatin accessibility (Table 1). Among them, 8 were ZNFs and 5 were long intergenic non-coding RNA (lincRNA) genes (Table 1).

The ZNF genes were further examined for gene expression and chromatin accessibility using the UCSC Genome Browser. Representative read tracks for ZNF626 highlight decreased gene expression and reduced chromatin accessibility in CHD7$^{-/+}$ and CHD7$^{-/-}$ hESC-DE cells as compared to CHD7$^{+/+}$ hESC-DE cells in a dose dependent manner (Fig. 4H). Differences in the gene expression and chromatin accessibility for some of the other ZNF genes are shown in Supplementary Figs. 10 and 11. Our results suggest that CHD7 regulates the chromatin landscape in hESC-DE cells by modifying chromatin accessibility at genes that are involved in generic transcription and other processes.

Among the genes that were highly down-regulated in both expression and chromatin accessibility in CHD7$^{-/-}$ hESC-DE cells, ZFPs have been reported to play a critical role in endoderm development [48–52]. STAG2 is also required for endoderm organ formation; STAG2-null embryos display developmental delay [53]. To confirm that STAG2 is required for DE development, we knocked down the STAG2 gene in hESCs by siRNA, which led to significantly reduced expression of STAG2 protein (Supplemental Fig. 12A). We then induced the hESCs to differentiate into DE and found that the generation of DE cells from STAG2 knockdown hESCs was reduced as compared to that from control hESCs (Supplemental

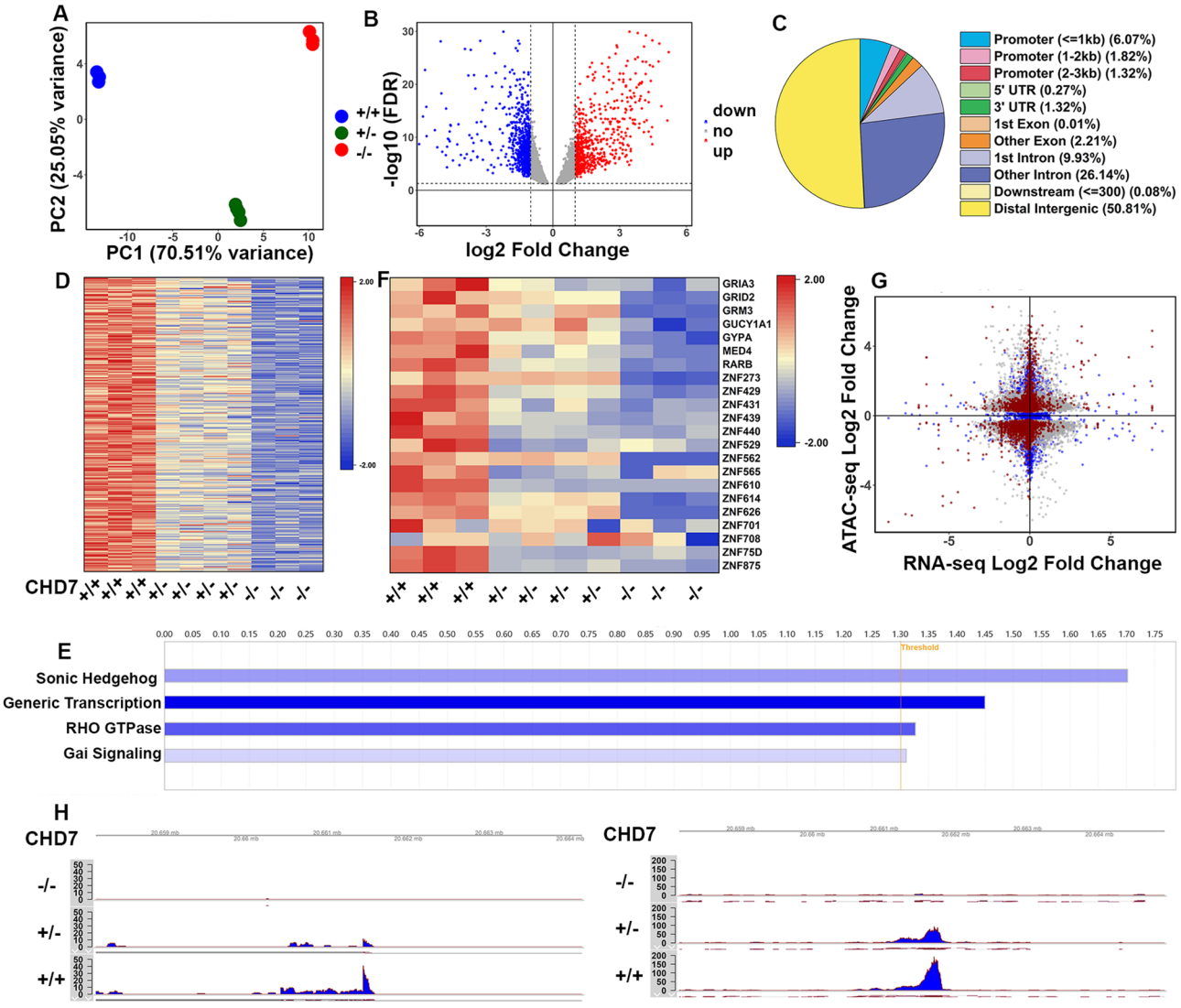

Fig. 4 CHD7 deletion affects chromatin accessibility in hESC-DE cells. CHD7$^{+/+}$, CHD7$^{+/-}$, and CHD7$^{-/-}$ hESCs were induced to differentiate into DE as in Fig. 2. On day 6, CXCR4^{+} DE cells were sorted from the cultures and subjected to ATAC-seq analysis. (**A**) PCA of ATAC-seq data showing PC1 and PC2 among CHD7$^{+/+}$, CHD7$^{+/-}$, and CHD7$^{-/-}$ hESC-DE groups. (**B**) Volcano plot showing chromatin accessibility changes between CHD7$^{+/+}$ and CHD7$^{-/-}$ hESC-DE groups. (**C**) Pie chart showing the distribution of differential peaks between CHD7$^{+/+}$ and CHD7$^{-/-}$ DE cells. (**D**) Heatmap showing significantly reduced chromatin accessibility in CHD7$^{-/-}$ and CHD7$^{+/-}$ hESC-DE cells as compared to CHD7$^{+/+}$ hESC-DE cells. The top 300 genes with significantly reduced chromatin accessibility in CHD7$^{-/-}$ hESC-DE cells are presented. The color scale is shown on the right. (**E**) IPA of reduced chromatin accessibility pathways in CHD7$^{-/-}$ hESC-DE cells compared to CHD7$^{+/+}$ hESC-DE cells. (**F**) Heatmap showing chromatin accessibility of genes related to the generic transcriptional pathway among CHD7$^{+/+}$, CHD7$^{+/-}$, and CHD7$^{-/-}$ hESC-DE groups. (**G**) Scatter plot showing genes/peaks from the combined analysis of the RNA-seq and ATAC-seq data. The x-axis is the log2 fold change in gene expression and the y-axis is the log2 fold change in peaks. Blue dot: RNA-seq; grey dot: ATAC-Seq; red dot: overlap genes. (**H**) Plot of RNA-seq and ATAC-seq read tracks along the gene body of ZNF626 using the UCSC Genome Bowser. The images show (left panel) decreased expression and (right panel) reduced chromatin accessibility of the enhancer region in CHD7$^{-/-}$ and CHD7$^{+/-}$ hESC-DE cells as compared to CHD7$^{+/+}$ hESC-DE cells. $n = 3$ CHD7$^{+/+}$, $n = 4$ CHD7$^{+/-}$, and $n = 3$ CHD7$^{-/-}$ group

Fig. 12B, C). The results suggest that STAG2 is required for DE development.

Deletion of CHD7 leads to reduced ability of hESCs to differentiate into mesoderm in vitro

Since CHARGE patients have multisystem developmental defects, we determined whether deletion of CHD7 also affected hESCs differentiation into mesoderm and ectoderm in vitro. An equal number of CHD7$^{+/-}$, CHD7$^{-/-}$ and CHD7$^{+/+}$ hESCs were induced to differentiate into mesoderm or ectoderm by the STEMdiff™ Trilineage Differentiation Kit. After differentiating into mesoderm, the cells were analyzed for expression of the mesoderm markers NKX2.5 and Brachyury by qRT-PCR. We found that the expression levels of the genes were decreased in CHD7$^{+/-}$and CHD7$^{-/-}$ hESC-derived cells

Table 1 Preeminent genes with different expression and chromatin accessibility in CHD7$^{-/-}$ hESC-DE cells

Gene	ATAC-seq			RNA-seq	
	Peak start position	log2 FC	FDR	log2 FC	padj
ZNF90	20,068,765	-1.698530007	9.67E-06	-1.05449	2.44E-14
ZNF626	20,661,484	-6.116337193	6.6E-34	-8.74297	5.87E-14
ZNF562	9,674,831	-5.743619371	1.96E-23	-7.29682	1.27E-26
ZNF440	11,813,983	-1.089788395	2.86E-14	-1.05657	4.83E-07
ZNF429	21,505,335	-1.035977432	7.84E-16	-1.28819	3.74E-11
ZNF283	43,827,130	-1.093467804	2.42E-13	-1.1946	5.1E-07
ZNF273	64,877,373	-1.286447443	1.92E-07	-1.09736	2.24E-08
ZNF229	44,448,305	-5.672527662	5.95E-11	-7.68805	6.75E-10
TRIM61	1.65E + 08	-2.247147827	3.52E-16	-2.87962	1.04E-09
TRIM4	99,919,409	-3.394881233	2.7E-11	-1.38217	1.52E-08
TMEM47	34,557,700	-1.010034608	0.001398	-1.56419	1.66E-20
TCEAL9	1.03E + 08	-1.09845557	1.1E-06	-1.00814	2.68E-10
SYT1	79,045,021	-1.598703802	1.63E-21	-1.84546	4.71E-14
STAG2	1.24E + 08	-1.207347434	0.000301	-1.1492	4.07E-13
SLC9A9	1.44E + 08	-1.282589016	4.64E-05	-1.23721	0.000119
SLC52A3	802,391	-3.679363308	1.97E-06	-1.19518	0.001781
RPS6KA6	84,078,969	-1.484448919	2.29E-05	-1.32439	8.01E-11
PURPL	27,472,020	-1.483748012	1.08E-21	-2.28822	1.84E-10
PNPLA4	7,927,182	-5.302758043	4.5E-12	-3.43741	4.64E-50
PCDH11X	92,100,300	-1.021491314	2.5E-05	-1.32419	9.89E-06
MOSPD1	1.35E + 08	-1.640325871	2.77E-08	-1.18812	3.63E-16
MOBP	39,577,489	-1.160033986	1.52E-14	-1.63032	6.35E-20
MAP3K13	1.85E + 08	-5.008396909	5.17E-19	-4.85978	1.65E-43
LSP1P4	91,659,872	-5.192845476	7.63E-09	-5.37987	5.49E-05
LINC02893	87,041,992	-1.133745654	0.000571	-2.46338	3.63E-07
LINC02523	1.26E + 08	-1.581612883	1.85E-09	-1.75761	0.002537
LINC01630	51,573,092	-1.090513227	6.5E-09	-1.01958	0.001882
LINC01139	2.38E + 08	-2.223362338	1.14E-30	-2.68756	4.78E-08
LINC00664	21,474,582	-4.402217427	1.15E-65	-4.44794	8.38E-13
KCNH5	62,781,330	-1.53917104	8.01E-08	-1.04036	0.003687
HS3ST5	1.14E + 08	-1.467550957	8.57E-08	-1.15776	0.002991
GRID2	92,444,186	-2.55949243	6.76E-23	-3.7928	8.48E-28
DMD	31,377,753	-2.082303185	4.63E-15	-1.75169	1.52E-26
D21S2088E	23,384,689	-1.905915798	3.08E-10	-5.64191	1.02E-07
CHRM3	2.39E + 08	-1.145468346	1.71E-06	-1.06806	0.000817
CCNO	55,263,447	-1.178882991	7.9E-06	-3.29862	8.73E-06
CASC9	75,324,281	-1.294708254	2.32E-10	-3.65368	4.67E-08
ARHGAP6	11,574,874	-2.386802252	4.63E-17	-1.73101	6.76E-05
ADGRL3	61,387,189	-1.494926255	5.08E-06	-1.50157	2.22E-12
ACSM4	7,304,529	-1.383830602	3.82E-09	-1.95812	6.78E-12

as compared to CHD7$^{+/+}$ hESCs in a dose-dependent manner (Fig. 5A, B). The data suggest that CHD7 is critical for mesoderm development from hESCs.

After the hESCs were induced to differentiate into ectoderm, we analyzed the cells for expression of the ectoderm markers Nestin and PAX6 by qRT-PCR. There were no significant differences in the expression levels of NESTIN and PAX6 among the CHD7$^{+/-}$, CHD7$^{-/-}$ and CHD7$^{+/+}$ hESC-derived cells (Fig. 5C, D). Our data suggest that CHD7 is not critical for ectoderm development from hESCs.

Discussion

We show here that loss of CHD7 did not affect the morphology, cell survival and proliferation of undifferentiated hESCs, which was consistent with other observations on mouse ESCs (mESCs) [17, 42]. We also did not observe significant changes in expression of hESC pluripotent markers, such as AP, SSEA4, OCT4 NANOG, and TRA-1-60R among CHD7$^{+/+}$, CHD7$^{+/-}$, and CHD7$^{-/-}$ undifferentiated hESCs, suggesting that CHD7 is not essential for the processes of hESC pluripotency and self-renewal. Our results are consistent with Schnetz's report showing

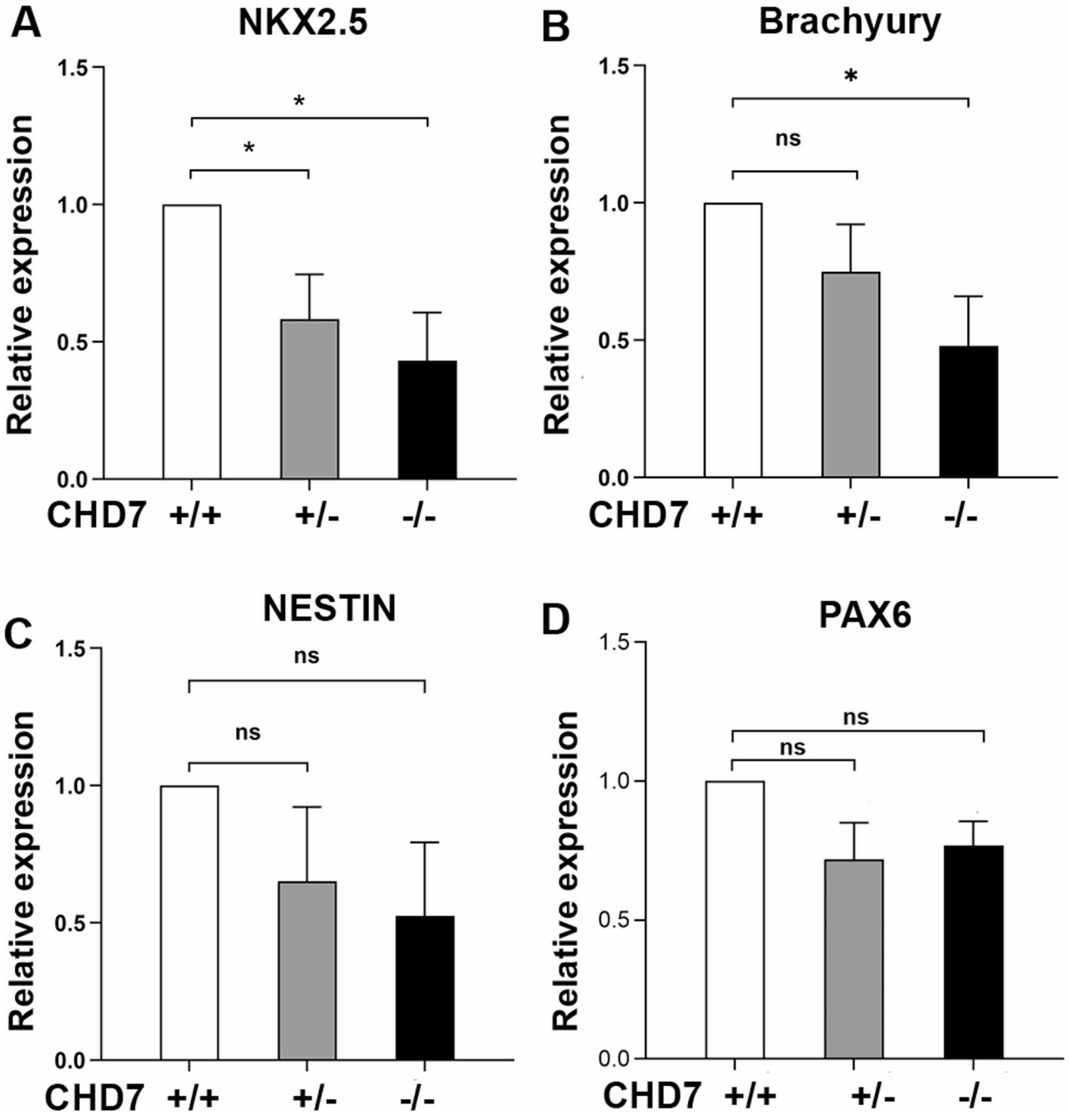

Fig. 5 CHD7 deficient hESCs have a defect in developing into mesoderm. CHD7$^{+/+}$, CHD7$^{+/-}$, and CHD7$^{-/-}$ hESCs (5×10^5 cells/well) were induced to differentiate into mesoderm or ectoderm by the STEMdiff™ Trilineage Differentiation Kit. After the differentiation, the cells were analyzed for the expression of the mesoderm markers (**A**) NKX2.5 and (**B**) Brachyury, as well as the ectoderm markers (**C**) NESTIN and (**D**) PAX6 by qRT-PCR. The data show relative expression levels; the expression level of each gene in CHD7$^{+/+}$ hESC-DE was defined as 1. The data are expressed as mean + SD from three independent experiments. * $P < 0.05$, compared with CHD7$^{+/-}$ or CHD7$^{+/+}$group; ns: no significant difference

that the expression levels of pluripotent markers between wild-type and CHD7 null mESCs are not significantly different [17]. Our results are also consistent with the data that CHD7 null mice die in mid-gestation, far beyond the ESC stage [24]. However, Yao et al. reported that there are subtle changes in expression of Oct4, Sox2, and Nanog between wild-type and CHD7 null mESCs [42]. Yamamoto et al. reported that CHD7 expression levels controlled the proliferation rate of undifferentiated hESCs [54]. The discrepancy among the studies may be due to the difference in cell lines, culture conditions, CHD7 deletion or downregulation methods and/or location, etc.

Although deletion of CHD7 did not affect undifferentiated hESC morphology, cell survival, proliferation, pluripotency and self-renewal, loss of CHD7 leads to reduced capacity to develop into DE. Like undifferentiated hESCs, loss of CHD7 does not affect the proliferation of hESC-DE. However, cell apoptosis of $CHD7^{+/-}$ and $CHD7^{-/-}$ hESC-DE was significantly higher than that of $CHD7^{+/+}$ hESC-DE and the effect is dosage dependent. In contrast, viable cells in $CHD7^{-/-}$ and $CHD7^{+/-}$ hESC-DE cells were significantly lower than those in $CHD7^{+/+}$ hESC-DE cells. The decreased survival of hESC-DE cells is likely to contribute to the reduced generation of DE from $CHD7^{+/-}$, and $CHD7^{-/-}$ hESCs.

CHARGE patients often have thymic hypo/aplasia, leading to T cell immunodeficiency. TECs are the major component of the thymic microenvironment for T cell development [27–35]. Zebrafish embryos with CHD7 knockdown or knockout have seriously impaired thymus development, and dramatic decrease of TECs and T cells [55]. Mice with heterozygous CHD7 mutant ($CHD7^{+/-}$) mice have thymic hypoplasia [24–26]. It has been reported that TECs originate from DE [36, 37]. Since we have shown that $CHD7^{+/-}$ or $CHD7^{-/-}$ hESCs have a reduced ability to develop into DE, it is likely that this contributes to thymic hypo/aplasia in CHARGE patients. It remains to be determined whether CHD7 is also involved in the development of TEPs and TECs from DE.

To investigate the mechanisms by which deletion of CHD7 leads to reduced DE development from hESCs, we compared global gene expression and genome wide mapping of chromatin accessibility among $CHD7^{+/+}$, $CHD7^{+/-}$, and $CHD7^{-/-}$ hESC-DE cells by RNA-seq and ATAC-seq. We have shown that loss of CHD7 leads to significant changes in the expression and chromatin accessibility of genes associated with several pathways. Among them, the generic transcription pathway was downregulated in both expression and chromatin accessibility, which is consistent with the results that CHD7 modulates chromatin configuration to regulate the temporal and spatial expression of genes during development [56].

By narrowing the integrated RNA-seq and ATAC-seq to the genes that were the most highly down-regulated in both expression and chromatin accessibility in $CHD7^{-/-}$ DE cells, we identified 40 genes (Table 1). Among them, 8 were ZNFs and 5 were lincRNA genes (Table 1). ZNFs play a critical role both in tissue homeostasis and disease. ZNFs have a wide range of molecular functions and are involved in regulating many cellular processes, including transcriptional regulation, protein degradation, signal transduction, DNA repair, and cell migration, etc [57]. ZNFs can also act as recruiters of chromatin modifiers, as co-factors, or as structural proteins [57]. LincRNAs can interact with various chromatin modifying complexes to modulate the chromatin state and have been implicated in differentiation and in developmental processes [58, 59]. Mice with lincRNA knockout had perinatal or postnatal lethal phenotypes, as well as growth and organ-restricted developmental defect phenotypes [60]. STAG2 is also one of the 40 genes that were highly downregulated in both expression and chromatin accessibility in $CHD7^{-/-}$ hESC-DE cells. We have shown that STAG2 knockdown in hESCs led to reduced generation of DE cells. CHARGE syndrome has multiple developmental anomalies; deregulation of ZNFs, lncRNAs and STAG2 caused by CHD7 mutations may play a key role in the defective organ development in CHARGE patients.

We have also shown that deletion of CHD7 leads to reduced development into mesoderm. The mesoderm gives rise to muscle cells and connective tissue in the body. It is likely that the defective mesoderm from CHD7 deficient hESCs also contributes to the multiple developmental disorders in CHARGE syndrome. In contrast, we did not observe significant changes in ectoderm development from CHD7 deficient hESCs. The ectoderm can differentiate into the nervous system, epidermis (skin and others) and various neural crest-derived tissues. Although nervous system abnormalities are common in CHARGE patients and CHD7 has been broadly implicated in wide areas of neurogenesis [61, 62], Yao et al. showed that loss of CHD7 did not affect the development of mESCs into $PAX6^{+}$ and $Nestin^{+}$ neural progenitor cells (NPCs) [42]. Our results are consistent with these results. It is likely that nervous system abnormalities observed in CHARGE patients are due to subsequent developmental defects from NPCs. Indeed, it has been reported that loss of CHD7 significantly reduced neuronal and glial differentiation from NPCs [42]. Similarly, CHD7 deletion did not affect oligodendrocyte precursor cells, but impaired their differentiation [46].

Conclusions

We have shown that loss of CHD7 leads to reduced ability to develop into DE and mesoderm in a dose-dependent manner, which is related to significant changes in the expression and chromatin accessibility of genes associated with several pathways. By combining RNA-seq and ATAC-seq data, we identified 40 genes that were highly down-regulated in both the expression and chromatin accessibility in CHD7 deleted hESC-DE cells. Our results provide new insights into the mechanisms by which CHD7 mutations cause multiple congenital anomalies.

Abbreviations

CHD7	Chromodomain helicase DNA-binding 7
DE	Definitive endoderm
hESCs	Human embryonic stem cells
mESCs	Mouse embryonic stem cells

RNA-seq	RNA sequencing
ATAC-seq	The assay for transposase-accessible chromatin with sequencing
TECs	Thymic epithelial cells (TECs)
TEPs	Thymic epithelial progenitors
ZNFs	Zinc finger proteins
lincRNA	Long intergenic non-coding RNA
gRNAs	Guide RNAs
qRT-PCR	Real-time qualitative RT-PCR
padj	Adjusted *P* value
FDR	False discovery rate
AP	Alkaline phosphatase
NPCs	Neural progenitor cells

Supplementary Information

The online version contains supplementary material available at https://doi.org/10.1186/s13287-025-04437-9.

Supplementary Material 1

Acknowledgements
We thank the Center for Genome Innovation and the Computational Biology Core in the Institute for Systems Genomics at the University of Connecticut for the RNA-seq experiments and data analysis. The authors declare that they have not used AI-generated work in this manuscript.

Author contributions
R.H, J.Z, K.C.L, S.W, J.Z, and C.S performed experiments. R.H, J.Z, and L.L analyzed data. R.H, J.Z, and L.L designed the study and drafted the manuscript. All authors read and approved of the final manuscript.

Funding
This work was supported by grants from NIH (R01AI175087 and R33AG072234).

Data availability
The datasets used and/or analyzed during the current study are available from the corresponding author on reasonable request. The RNA-seq and ATAC-seq data have been deposited in the NCBI GEO database under accession number GSE275739 and GSE275741.

Declarations

Ethics approval and consent to participate
The H9 hESCs were obtained from the WiCell Research Institute under a material transfer agreement (WeCell Agreement No. 12-WO0384). The hESCs were used according to a protocol titled "Treating T cell immunodeficiency in CHARGE syndrome by ESC- and iPSC-derived thymic epithelial cells" approved by the Stem Cell Research Oversight Committee at the University of Connecticut (SCRO #2023-2, approval day 2/23/2023).

Consent for publication
Not applicable.

Competing interests
The authors declare no competing interests.

Received: 30 August 2024 / Accepted: 10 June 2025
Published online: 17 June 2025

References

1. Jyonouchi S, McDonald-McGinn DM, Bale S, Zackai EH, Sullivan KE. CHARGE (coloboma, heart defect, Atresia choanae, retarded growth and development, genital hypoplasia, ear anomalies/deafness) syndrome and chromosome 22q11.2 deletion syndrome: a comparison of Immunologic and nonimmunologic phenotypic features. Pediatrics. 2009;123(5):e871–7.
2. Zentner GE, Layman WS, Martin DM, Scacheri PC. Molecular and phenotypic aspects of CHD7 mutation in CHARGE syndrome. Am J Med Genet A. 2010;152a(3):674–86.
3. van Ravenswaaij-Arts C, Martin DM. New insights and advances in CHARGE syndrome: diagnosis, etiologies, treatments, and research discoveries. Am J Med Genet Part C Seminars Med Genet. 2017;175(4):397–406.
4. Janssen N, Bergman JE, Swertz MA, Tranebjaerg L, Lodahl M, Schoots J, et al. Mutation update on the CHD7 gene involved in CHARGE syndrome. Hum Mutat. 2012;33(8):1149–60.
5. Jongmans MC, Admiraal RJ, van der Donk KP, Vissers LE, Baas AF, Kapusta L, et al. CHARGE syndrome: the phenotypic spectrum of mutations in the CHD7 gene. J Med Genet. 2006;43(4):306–14.
6. Lalani SR, Safiullah AM, Fernbach SD, Harutyunyan KG, Thaller C, Peterson LE, et al. Spectrum of CHD7 mutations in 110 individuals with CHARGE syndrome and genotype-phenotype correlation. Am J Hum Genet. 2006;78(2):303–14.
7. Pagon RA, Graham JM Jr., Zonana J, Yong SL. Coloboma, congenital heart disease, and choanal Atresia with multiple anomalies: CHARGE association. J Pediatr. 1981;99(2):223–7.
8. Assing K, Nielsen C, Kirchhoff M, Madsen HO, Ryder LP, Fisker N. CD4 + CD31 + recent thymic emigrants in CHD7 haploinsufficiency (CHARGE syndrome): a case. Hum Immunol. 2013;74(9):1047–50.
9. Chopra C, Baretto R, Duddridge M, Browning MJ. T-cell immunodeficiency in CHARGE syndrome. Acta Paediatr (Oslo Norway: 1992). 2009;98(2):408–10.
10. Mehr S, Hsu P, Campbell D. Immunodeficiency in CHARGE syndrome. Am J Med Genet Part C Seminars Med Genet. 2017;175(4):516–23.
11. Wong MT, Lambeck AJ, van der Burg M, la, Bastide-van Gemert S, Hogendorf LA, van Ravenswaaij-Arts CM et al. Immune Dysfunction in Children with CHARGE Syndrome: A Cross-Sectional Study. PloS one. 2015;10(11):e0142350.
12. Writzl K, Cale CM, Pierce CM, Wilson LC, Hennekam RC. Immunological abnormalities in CHARGE syndrome. Eur J Med Genet. 2007;50(5):338–45.
13. Wong MT, Scholvinck EH, Lambeck AJ, van Ravenswaaij-Arts CM. CHARGE syndrome: a review of the immunological aspects. Eur J Hum Genetics: EJHG. 2015;23(11):1451–9.
14. Zentner GE, Hurd EA, Schnetz MP, Handoko L, Wang C, Wang Z, et al. CHD7 functions in the nucleolus as a positive regulator of ribosomal RNA biogenesis. Hum Mol Genet. 2010;19(18):3491–501.
15. Vissers LE, van Ravenswaaij CM, Admiraal R, Hurst JA, de Vries BB, Janssen IM, et al. Mutations in a new member of the chromodomain gene family cause CHARGE syndrome. Nat Genet. 2004;36(9):955–7.
16. Bergman JE, Janssen N, Hoefsloot LH, Jongmans MC, Hofstra RM, van Ravenswaaij-Arts CM. CHD7 mutations and CHARGE syndrome: the clinical implications of an expanding phenotype. J Med Genet. 2011;48(5):334–42.
17. Schnetz MP, Handoko L, Akhtar-Zaidi B, Bartels CF, Pereira CF, Fisher AG, et al. CHD7 targets active gene enhancer elements to modulate ES cell-specific gene expression. PLoS Genet. 2010;6(7):e1001023.
18. Yan S, Thienthanasit R, Chen D, Engelen E, Brühl J, Crossman DK, et al. CHD7 regulates cardiovascular development through ATP-dependent and -independent activities. Proc Natl Acad Sci USA. 2020;117(46):28847–58.
19. Kim HG, Kurth I, Lan F, Meliciani I, Wenzel W, Eom SH, et al. Mutations in CHD7, encoding a chromatin-remodeling protein, cause idiopathic hypogonadotropic hypogonadism and Kallmann syndrome. Am J Hum Genet. 2008;83(4):511–9.
20. Sanka M, Tangsinmankong N, Loscalzo M, Sleasman JW, Dorsey MJ. Complete digeorge syndrome associated with CHD7 mutation. J Allergy Clin Immunol. 2007;120(4):952–4.
21. Gonçalves CI, Patriarca FM, Aragüés JM, Carvalho D, Fonseca F, Martins S, et al. High frequency of CHD7 mutations in congenital hypogonadotropic hypogonadism. Sci Rep. 2019;9(1):1597.
22. Corsten-Janssen N, Saitta SC, Hoefsloot LH, McDonald-McGinn DM, Driscoll DA, Derks R, et al. More clinical overlap between 22q11.2 deletion syndrome and CHARGE syndrome than often anticipated. Mol Syndromol. 2013;4(5):235–45.
23. Schnetz MP, Bartels CF, Shastri K, Balasubramanian D, Zentner GE, Balaji R, et al. Genomic distribution of CHD7 on chromatin tracks H3K4 methylation patterns. Genome Res. 2009;19(4):590–601.
24. Bosman EA, Penn AC, Ambrose JC, Kettleborough R, Stemple DL, Steel KP. Multiple mutations in mouse Chd7 provide models for CHARGE syndrome. Hum Mol Genet. 2005;14(22):3463–76.
25. Hurd EA, Capers PL, Blauwkamp MN, Adams ME, Raphael Y, Poucher HK, et al. Loss of Chd7 function in gene-trapped reporter mice is embryonic lethal

and associated with severe defects in multiple developing tissues. Mamm Genome. 2007;18(2):94–104.
26. Randall V, McCue K, Roberts C, Kyriakopoulou V, Beddow S, Barrett AN, et al. Great vessel development requires biallelic expression of Chd7 and Tbx1 in pharyngeal ectoderm in mice. J Clin Invest. 2009;119(11):3301–10.
27. Chidgey A, Dudakov J, Seach N, Boyd R. Impact of niche aging on thymic regeneration and immune reconstitution. Semin Immunol. 2007;19(5):331–40.
28. Anderson G, Takahama Y. Thymic epithelial cells: working class heroes for T cell development and repertoire selection. Trends Immunol. 2012;33(6):256–63.
29. Zediak VP, Bhandoola A. Aging and T cell development: interplay between progenitors and their environment. Semin Immunol. 2005;17(5):337–46.
30. Ciofani M, Zuniga-Pflucker JC. The thymus as an inductive site for T lymphopoiesis. Annu Rev Cell Dev Biol. 2007;23:463–93.
31. Mondino A, Khoruts A, Jenkins MK. The anatomy of T-cell activation and tolerance. Proc Natl Acad Sci USA. 1996;93(6):2245–52.
32. Houssaint E, Flajnik M. The role of thymic epithelium in the acquisition of tolerance. Immunol Today. 1990;11(10):357–60.
33. Dudakov JA, Hanash AM, Jenq RR, Young LF, Ghosh A, Singer NV, et al. Interleukin-22 drives endogenous thymic regeneration in mice. Sci (New York NY). 2012;336(6077):91–5.
34. Beaudette-Zlatanova BC, Knight KL, Zhang S, Stiff PJ, Zúñiga-Pflücker JC, Le PT. A human thymic epithelial cell culture system for the promotion of lymphopoiesis from hematopoietic stem cells. Exp Hematol. 2011;39(5):570–9.
35. Min D, Panoskaltsis-Mortari A, Kuro OM, Holländer GA, Blazar BR, Weinberg KI. Sustained thymopoiesis and improvement in functional immunity induced by exogenous KGF administration in murine models of aging. Blood. 2007;109(6):2529–37.
36. Gordon J, Wilson VA, Blair NF, Sheridan J, Farley A, Wilson L, et al. Functional evidence for a single endodermal origin for the thymic epithelium. Nat Immunol. 2004;5(5):546–53.
37. Bleul CC, Corbeaux T, Reuter A, Fisch P, Monting JS, Boehm T. Formation of a functional thymus initiated by a postnatal epithelial progenitor cell. Nature. 2006;441(7096):992–6.
38. Lai L, Jin J. Generation of thymic epithelial cell progenitors by mouse embryonic stem cells. Stem Cells. 2009;27(12):3012–20.
39. Zhao J, Hu R, Lai KC, Zhang Z, Lai L. Recombinant FOXN1 fusion protein increases T cell generation in old mice. Front Immunol. 2024;15:1423488.
40. Yan Y, Su M, Song Y, Tang Y, Tian C, Rood D et al. Tbx1 modulates endodermal and mesodermal differentiation from mouse induced pluripotent stem cells. Stem Cells Dev. 2014.
41. Lin Y, Cui C, Su M, Tian X, Huang Y, Zhao J, et al. Skint8, a novel B7 Family-Related molecule, negatively regulates T cell responses. J Immunol (Baltimore Md: 1950). 2019;203(2):400–7.
42. Yao H, Hannum DF, Zhai Y, Hill SF, Albanus RD, Lou W, et al. CHD7 promotes neural progenitor differentiation in embryonic stem cells via altered chromatin accessibility and nascent gene expression. Sci Rep. 2020;10(1):17445.
43. Whittaker DE, Riegman KL, Kasah S, Mohan C, Yu T, Pijuan-Sala B, et al. The chromatin remodeling factor CHD7 controls cerebellar development by regulating reelin expression. J Clin Invest. 2017;127(3):874–87.
44. Feng W, Kawauchi D, Körkel-Qu H, Deng H, Serger E, Sieber L, et al. Chd7 is indispensable for mammalian brain development through activation of a neuronal differentiation programme. Nat Commun. 2017;8:14758.
45. Bouazoune K, Kingston RE. Chromatin remodeling by the CHD7 protein is impaired by mutations that cause human developmental disorders. Proc Natl Acad Sci USA. 2012;109(47):19238–43.
46. He D, Marie C, Zhao C, Kim B, Wang J, Deng Y, et al. Chd7 cooperates with Sox10 and regulates the onset of CNS myelination and remyelination. Nat Neurosci. 2016;19(5):678–89.
47. Hnisz D, Abraham BJ, Lee TI, Lau A, Saint-André V, Sigova AA, et al. Super-enhancers in the control of cell identity and disease. Cell. 2013;155(4):934–47.
48. Fang Y, Li X. Metabolic and epigenetic regulation of endoderm differentiation. Trends Cell Biol. 2022;32(2):151–64.
49. Chia CY, Madrigal P, Denil S, Martinez I, Garcia-Bernardo J, El-Khairi R, et al. GATA6 cooperates with EOMES/SMAD2/3 to deploy the gene regulatory network governing human definitive endoderm and pancreas formation. Stem Cell Rep. 2019;12(1):57–70.
50. Tiyaboonchai A, Cardenas-Diaz FL, Ying L, Maguire JA, Sim X, Jobaliya C, et al. GATA6 plays an important role in the induction of human definitive endoderm, development of the pancreas, and functionality of pancreatic β cells. Stem Cell Rep. 2017;8(3):589–604.
51. García-García MJ, Shibata M, Anderson KV. Chato, a KRAB zinc-finger protein, regulates convergent extension in the mouse embryo. Development. 2008;135(18):3053–62.
52. Patterson ES, Addis RC, Shamblott MJ, Gearhart JD. SOX17 directly activates Zfp202 transcription during in vitro endoderm differentiation. Physiol Genomics. 2008;34(3):277–84.
53. De Koninck M, Lapi E, Badía-Careaga C, Cossío I, Giménez-Llorente D, Rodríguez-Corsino M, et al. Essential roles of cohesin STAG2 in mouse embryonic development and adult tissue homeostasis. Cell Rep. 2020;32(6):108014.
54. Yamamoto T, Takenaka C, Yoda Y, Oshima Y, Kagawa K, Miyajima H, et al. Differentiation potential of pluripotent stem cells correlates to the level of CHD7. Sci Rep. 2018;8(1):241.
55. Liu ZZ, Wang ZL, Choi TI, Huang WT, Wang HT, Han YY, et al. Chd7 is critical for early T-Cell development and Thymus organogenesis in zebrafish. Am J Pathol. 2018;188(4):1043–58.
56. Marie C, Clavairoly A, Frah M, Hmidan H, Yan J, Zhao C, et al. Oligodendrocyte precursor survival and differentiation requires chromatin remodeling by Chd7 and Chd8. Proc Natl Acad Sci USA. 2018;115(35):E8246–55.
57. Cassandri M, Smirnov A, Novelli F, Pitolli C, Agostini M, Malewicz M, et al. Zinc-finger proteins in health and disease. Cell Death Discovery. 2017;3(1):17071.
58. Deniz E, Erman B. Long noncoding RNA (lincRNA), a new paradigm in gene expression control. Funct Integr Genom. 2017;17(2):135–43.
59. Ransohoff JD, Wei Y, Khavari PA. The functions and unique features of long intergenic non-coding RNA. Nat Rev Mol Cell Biol. 2018;19(3):143–57.
60. Sauvageau M, Goff LA, Lodato S, Bonev B, Groff AF, Gerhardinger C, et al. Multiple knockout mouse models reveal LincRNAs are required for life and brain development. eLife. 2013;2:e01749.
61. Feng W, Shao C, Liu HK. Versatile roles of the chromatin remodeler CHD7 during brain development and disease. Front Mol Neurosci. 2017;10:309.
62. Bajpai R, Chen DA, Rada-Iglesias A, Zhang J, Xiong Y, Helms J, et al. CHD7 cooperates with PBAF to control multipotent neural crest formation. Nature. 2010;463(7283):958–62.

Publisher's note